JCI The Journal of Clinical Investigation

Synaptic pathology and therapeutic repair in adult retinoschisis mouse by AAV-*RS1* transfer

Jingxing Ou, … , Wei Li, Paul A. Sieving

J Clin Invest. 2015;125(7):2891-2903. https://doi.org/10.1172/JCI81380.

Research Article **Ophthalmology**

Strategies aimed at invoking synaptic plasticity have therapeutic potential for several neurological conditions. The human retinal synaptic disease X-linked retinoschisis (XLRS) is characterized by impaired visual signal transmission through the retina and progressive visual acuity loss, and mice lacking retinoschisin (RS1) recapitulate human disease. Here, we demonstrate that restoration of RS1 via retina-specific delivery of adeno-associated virus type 8-*RS1* (AAV8-*RS1*) vector rescues molecular pathology at the photoreceptor–depolarizing bipolar cell (photoreceptor-DBC) synapse and restores function in adult *Rs1*-KO animals. Initial development of the photoreceptor-DBC synapse was normal in the*Rs1*-KO retina; however, the metabotropic glutamate receptor 6/transient receptor potential melastatin subfamily M member 1–signaling (mGluR6/TRPM1-signaling) cascade was not properly maintained. Specifically, the TRPM1 channel and G proteins Gαo, Gβ5, and RGS11 were progressively lost from postsynaptic DBC dendritic tips, whereas the mGluR6 receptor and RGS7 maintained proper synaptic position. This postsynaptic disruption differed from other murine night-blindness models with an electronegative electroretinogram response, which is also characteristic of murine and human XLRS disease. Upon AAV8-*RS1* gene transfer to the retina of adult XLRS mice, TRPM1 and the signaling molecules returned to their proper dendritic tip location, and the DBC resting membrane potential was restored. These findings provide insight into the molecular plasticity of a critical synapse in the visual system and demonstrate potential therapeutic avenues for some diseases involving synaptic pathology.

Synaptic pathology and therapeutic repair in adult retinoschisis mouse by AAV-*RS1* transfer

Jingxing Ou,[1] Camasamudram Vijayasarathy,[2] Lucia Ziccardi,[2] Shan Chen,[1] Yong Zeng,[2] Dario Marangoni,[2] Jodie G. Pope,[1] Ronald A. Bush,[2] Zhijian Wu,[3] Wei Li,[1] and Paul A. Sieving[2,4]

[1]Retinal Neurobiology Section, National Eye Institute, [2]Section on Translational Research for Retinal and Macular Degeneration, National Institute on Deafness and Other Communication Disorders, [3]Ocular Gene Therapy Core, National Eye Institute, and [4]National Eye Institute, NIH, Bethesda, Maryland, USA.

Strategies aimed at invoking synaptic plasticity have therapeutic potential for several neurological conditions. The human retinal synaptic disease X-linked retinoschisis (XLRS) is characterized by impaired visual signal transmission through the retina and progressive visual acuity loss, and mice lacking retinoschisin (RS1) recapitulate human disease. Here, we demonstrate that restoration of RS1 via retina-specific delivery of adeno-associated virus type 8-*RS1* (AAV8-*RS1*) vector rescues molecular pathology at the photoreceptor–depolarizing bipolar cell (photoreceptor-DBC) synapse and restores function in adult *Rs1*-KO animals. Initial development of the photoreceptor-DBC synapse was normal in the *Rs1*-KO retina; however, the metabotropic glutamate receptor 6/transient receptor potential melastatin subfamily M member 1–signaling (mGluR6/TRPM1-signaling) cascade was not properly maintained. Specifically, the TRPM1 channel and G proteins Gαo, Gβ5, and RGS11 were progressively lost from postsynaptic DBC dendritic tips, whereas the mGluR6 receptor and RGS7 maintained proper synaptic position. This postsynaptic disruption differed from other murine night-blindness models with an electronegative electroretinogram response, which is also characteristic of murine and human XLRS disease. Upon AAV8-*RS1* gene transfer to the retina of adult XLRS mice, TRPM1 and the signaling molecules returned to their proper dendritic tip location, and the DBC resting membrane potential was restored. These findings provide insight into the molecular plasticity of a critical synapse in the visual system and demonstrate potential therapeutic avenues for some diseases involving synaptic pathology.

Introduction

A number of neurological diseases involve synaptic pathology, including myasthenia gravis, from autoimmune attack on the motor synapse; Parkinson's disease, from degeneration of dopaminergic neurons; and intellectual development disorders, such as autism and fragile X syndrome, that result from mutations in genes that support the development and structure of synapses. A possible therapeutic strategy would be to invoke innate synaptic plasticity to strengthen the channels or increase their numbers. Several recent studies have tested the feasibility of this approach to remodeling synaptic structure and improving function in neurodevelopmental disorders. In a nonhuman primate model of Parkinson's disease, injection of a viral vector encoding 3 genes for dopamine synthesis into the striatum safely restored extracellular concentrations of dopamine and corrected the motor deficits (1). Other examples of inducing neurosynaptic plasticity for therapy include reversal of depressed behaviors in mice by serotonin receptor–binding protein (p11) gene therapy into brain regions within the reward circuit of *P11*-knockout mice (2) and restoration of hearing by virally mediated vesicular glutamate transporter 3 (*Vglut3*) gene therapy in *Vglut3*-KO mice (3). We now demonstrate therapeutic synaptic repair is possible in the adult murine model of the retinal disease X-linked retinoschisis (XLRS).

XLRS is a rare but readily recognized ocular pathological condition that causes splitting through the retinal layers (4, 5). The appearance of cysts in the retina first caught the attention of Josef Haas when he described this clinical condition in 2 young boys in 1898 (6). This was eventually recognized as an X-linked condition affecting only males (7, 8). Retinoschisin (*RS1*) gene underlying the cause of this retinal splitting and early vision loss was later identified on the X chromosome and shown to encode a 224–amino acid RS1 protein with a conserved discoidin motif sequence implicated in cell adhesion (9–11). In adult retina, RS1 is predominantly expressed and secreted from photoreceptor and bipolar cells (BCs) (12, 13). As an extracellular matrix (ECM) and cell-adhesion molecule, RS1 was proposed to preserve the structure and function of the retina (11). The schisis pathology observed in XLRS patients is consistent with loss of RS1 function as a cellular adhesive (4, 5). For the most part, medical attention has focused on the physical splitting of retinal layers and the intraretinal cavities, known as "retinoschisis," filled with intraretinal fluid. Treatment has been attempted using carbonic anhydrase inhibitors (2% topical dorzolamide), which are effective in several conditions involving cystoid macular edema (14). While this treatment reduced the schisis cavities, it did not necessarily correlate with improvement in visual acuity (15, 16). *Rs1*-KO mouse models reproduce the human XLRS disease phenotype and have been used to understand the cellular and molecular mechanisms of disease (11, 17, 18).

▶ Related Commentary: p. 2572

Authorship note: Jingxing Ou and Camasamudram Vijayasarathy are co–first authors.
Conflict of interest: The authors have declared that no conflict of interest exists.
Submitted: February 9, 2015; **Accepted:** April 30, 2015.
Reference information: *J Clin Invest*. 2015;125(7):2891–2903. doi:10.1172/JCI81380.

Table 1. A comparison of synaptic abnormalities in *Rs1*-KO, *Rd1*, and ERG b-wave mutant mouse models

Reference	Genotype	mGluR6	TRPM1	RGS7	RGS11	Gαo	Gβ5	Gβ3	GPR179	Nyctalopin
Present study	*Rs1*$^{-/-}$	Normal	Reduced at OPL	Normal	Mislocalized/ expanded	Mislocalized/ expanded	Mislocalized/ expanded	NT	Reduced in adults	NT
21	*mGluR6*$^{-/-}$	Null	Reduced at OPL	Reduced	Reduced at OPL	Normal	Reduced at OPL	Normal	Normal	NT
29	*NYX*^{nob}	Normal	Absent at OPL	NT	NT	NT	NT	NT	Normal	Null
24	*Trpm1*$^{-/-}$	Normal	Null	NT	NT	NT	NT	NT	Normal	Normal
50	*GPR179*^{nob5}	Normal	Normal	Mislocalized	Mislocalized	NT	Mislocalized	NT	Null	Normal
25	*Gαo*$^{-/-}$	Normal	NT	NT	NT	Null	NT	NT	NT	NT
46	*Pde6b*^{Rd1}	Reduced	Mislocalized	NT	NT	NT	NT	NT	NT	NT
28	*RGS11*$^{-/-}$	Normal	Normal	No noticeable effect	Null	NT	No noticeable effect	NT	Normal	Normal
28	*RGS7*$^{-/-}$	Normal	Normal	Null	No effect	NT	No effect	NT	Normal	Normal
45	*Nob2*	Reduced at OPL, mislocalized	NT	NT	NT	NT	NT	NT	NT	NT

NT, not tested.

Another feature of XLRS disease is reduced electroretinogram (ERG) b-wave amplitude (4, 5). The b-wave reflects light-dependent retinal activity and synaptic activation of depolarizing ON-BCs via the G protein–coupled heterotrimeric metabotropic glutamate receptor 6 (mGluR6), raising a suspicion of synaptic failure in XLRS disease (19). The molecular and cellular processes that support ERG b-wave generation in depolarizing bipolar cells (DBCs) have been well characterized. In this pathway, mGluR6 (20, 21) regulates the activity of a nonselective cation channel, transient receptor potential melastatin subfamily M member 1 (TRPM1) (22–24), via a heterotrimeric G_O protein subunit Gαo (25). Other accessory proteins include Gβ5, a member of the heterotrimeric G protein β subunit family (26), the regulators of G protein signaling (RGS) RGS7 and RGS11 (27, 28), and the scaffolding protein nyctalopin, a product of the *NYX* gene (29, 30). Gαo and TRPM1, as well as the Gβ5-RGS complexes, all colocalize with mGluR6 at the dendritic tips of depolarizing ON-BCs (30, 31). The sequence of ON-BC events, in brief, is as follows: (a) in darkness, glutamate released from photoreceptor terminals binds to mGluR6 to activate G protein $Go_{\alpha\beta\gamma}$, which (b) leads to exchange of Gαo-bound GDP for GTP; then (c) the dissociation of the activated $G\alpha o_{GTP}$ from βγ subunits (d) in GTP-bound state Gαo closes constitutively active TRPM1 channels, which hyperpolarize and deactivate ON-BCs. Conversely, in light, (a) a decrease in glutamate binding to mGluR6 terminates G protein signaling by hydrolysis of the Gαo-bound GTP to GDP and (b) opens TRPM1 channels to allow flow of cation current, thus causing (c) the ON-BCs to depolarize. The intrinsic rates of GTP hydrolysis by Gαo are slow, requiring tens of seconds. The Gβ5-RGS7 and Gβ5-RGS11 complexes regulate synaptic kinetics (speed) and duration of ON-DBC light responses by accelerating hydrolysis of Gαo-bound GTP to GDP to inactivate signaling (28, 32).

In this study, we used immunohistochemistry in conjunction with biochemical and physiological methods to analyze the molecular and cellular processes that support ERG b-wave generation, namely, presynaptic photoreceptor molecules involved in glutamate release and components of mGluR6-signaling cascade in *Rs1*-KO mice before and following adeno-associated virus type 8–mediated gene transfer (AAV8-*RS1*). We found a failure of synaptic maintenance that accounts for the progressive retinal-signaling dysfunction in XLRS. The RS1 protein deficiency in XLRS causes a unique pattern of synaptic molecular failure different from that of other murine models of synaptic dysfunction that limit vision in congenital stationary night blindness–type (CSNB-type) disorders (Table 1). We found that molecular pathology could be reversed upon provision of the RS1 protein by gene transfer to the adult XLRS mouse retina and that this restored the normal resting potential of the DBC membrane. This demonstrates that synaptic plasticity and repair can be invoked for therapeutic benefit even in postdevelopmental adult mammalian retina.

Results

Structural and functional synapse anomalies in young Rs1-KO mice. RS1 expression in P22 WT mouse retina is greatest in photoreceptor inner segments and in BCs (Figure 1A). Confocal images with RS1 and Gαo antibodies show an overlapping staining pattern in postsynaptic BC dendritic shafts, with Gαo signals concentrating tightly at the dendritic tips in the outer plexiform layer (OPL) (Figure 1, A–D). On the presynaptic side, RIBEYE and Bassoon are present at the synaptic ribbon (33), and they are closely associated and form the horseshoe-shaped presynaptic complex in both WT and *Rs1*-KO retinas (Figure 2, A–H). Immunolabeling the α1F subunit of the voltage-dependent calcium channel complex (Cav1.4/CACNA1F) showed it juxtaposed to RIBEYE at the OPL of both WT and *Rs1*-KO retina (Figure 1, E and F). In general, at P22, there were no significant alternations in the expression levels and localization of presynaptic proteins, including the VGluT1 (34), which loads glutamate into synaptic vesicles (Figure 2, M–T, and Supplemental Figure 1; supplemental material available online with this article; doi:10.1172/JCI81380DS1). Many of the postsynaptic proteins are also present and are largely striated at the synaptic layer normally, as shown in retinal whole mounts (Figure 2, A–H: mGluR6) and retinal cross

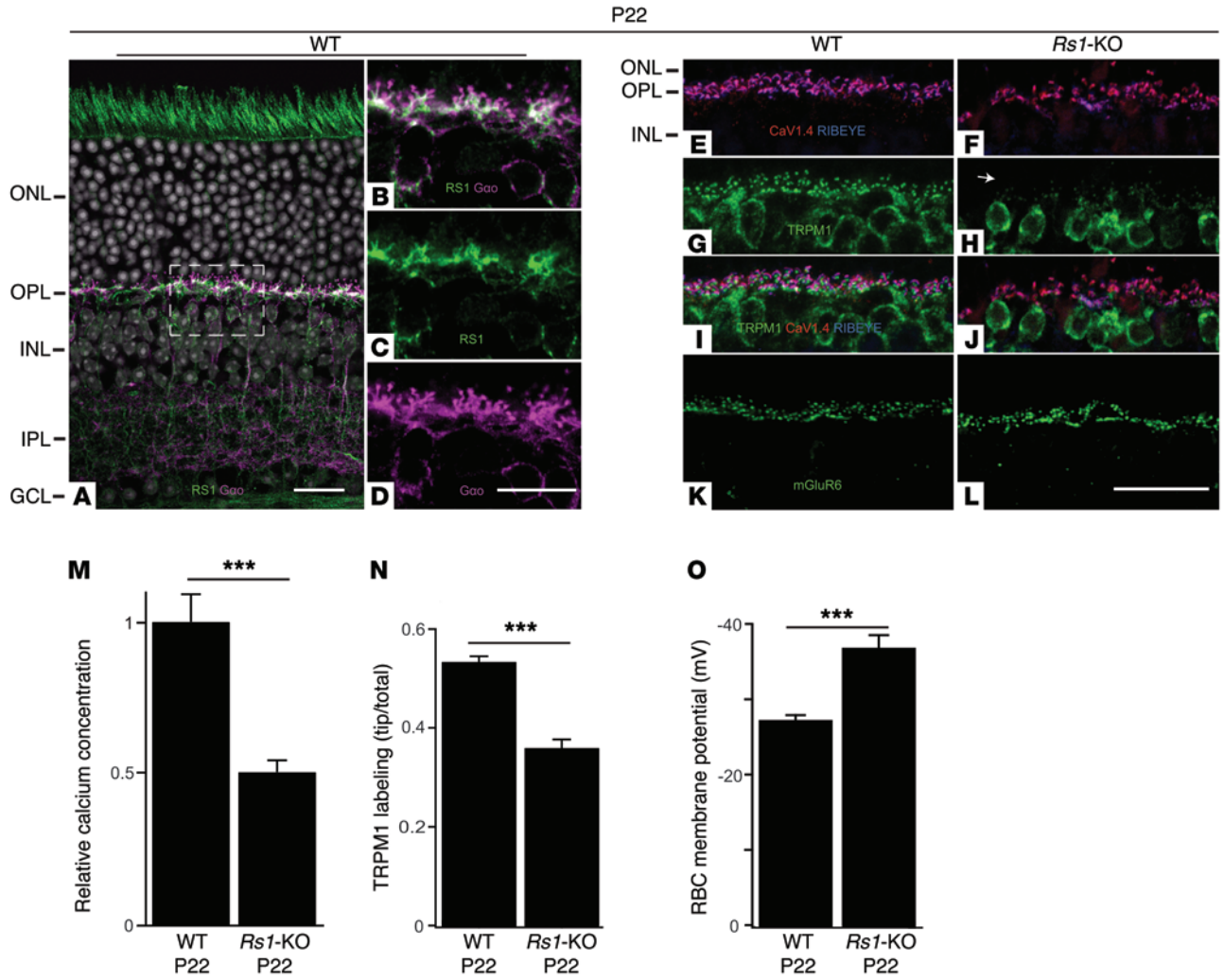

Figure 1. Photoreceptor synaptic calcium deficiency and bipolar TRPM1 channel anomaly and hyperpolarized MP in P22 *Rs1*-KO retinas. (**A**–**D**) RS1 (green); counterstain Gαo (purple), a BC marker. In WT retina, Rs1 is profusely present in the photoreceptor inner segments and OPL. Rs1 is concentrated at the ON-BC dendritic shaft and sparsely present around the cell soma. (**E** and **F**) In *Rs1*-KO retinas at P22, presynaptic RIBEYE (blue) and CaV1.4 (red) are normally distributed as in WT. In contrast to WT retinas (**G**) where TRPM1 (green) proteins are aggregated at the dendritic tips opposing the presynaptic RIBEYE/CaV1.4 complex (**I**), the dendritic component of TRPM1 is greatly diminished (**H**, arrow, and **J**) in *Rs1*-KO retinas. (**K**–**L**) At P22, mGluR6 (green) is exclusively located at the dendritic tips of the ON-BCs in both WT and *Rs1*-KO retinas. (**M**) At P22, measurements with Ca^{2+}-sensitive dye fluo-4 showed that the median $[Ca^{2+}]i$ in *Rs1*-KO rod spherules was 48% of normalized median WT value ($n = 7$; $^{***}P < 0.001$; Student's *t* test). (**N**) TRPM1 signal intensity at the bipolar dendritic tips was 36% of the whole-cell signal in *Rs1*-KO retinas, significantly lower than that of over 53% in WT ($n = 5$; $^{***}P < 0.001$; Student's *t* test). (**O**) In line with the TRPM1 defects, the MP of light-exposed RBC is abnormally low in light-exposed *Rs1*-KO retinas ($n = 5$; $^{***}P < 0.001$; Student's *t* test). GCL, ganglion cell layer. Scale bars: 10 μm (**B**–**D**); 20 μm (**A**, **E**–**L**). $n = 4$.

sections (Figure 2, I–X: Gαo, Gβ5, RGS11, and RGS7). These results indicate that the synaptic structures develop normally and are largely intact in the *Rs1*-KO retina at this young age.

However, even at P22, live-cell Ca^{2+} imaging measurement showed low basal Ca^{2+} concentration levels in photoreceptor synaptic terminals in retina slices. As with other neurons, photoreceptor synaptic transmission is tightly regulated by Ca^{2+} influx through voltage-dependent calcium channels and the intracellular Ca^{2+} concentration ($[Ca^{2+}]i$) (35, 36). These experiments were performed with dim background illumination (mesopic range), whereby calcium channels would be activated but not at the peak. Mean $[Ca^{2+}]i$ in *Rs1*-KO rod synaptic terminals was only 48% of WT at P22 ($n = 7$; $P < 0.001$; Student's *t* test) (Figure 1M). Although the ribbon synapse structure and calcium channels at the active zone are intact in the *Rs1*-KO mouse, the abnormally low $[Ca^{2+}]i$ in photoreceptor terminals indicates that presynaptic function is disrupted by absence of RS1 protein expression.

For postsynaptic structure, we focused on mGluR6, TRPM1, and the associated signaling cascade proteins at P22. In retinal cross sections and on flat mount preparation, mGluR6 was expressed on the dendritic tips of ON-BCs, albeit the overall distribution was slightly disorganized in the *Rs1*-KO retina (Figure 1, K and L, and Figure 2, A–H). Nonetheless, the mGluR6 receptor puncta were located appropriately, immediately adjacent to presynaptic ribbons (Figure 2, E–H). TRPM1 position was grossly disrupted, however. Normally in WT retinas, TRPM1 labeling heavily decorates the BC dendritic tips in the OPL as bright puncta, with lighter staining in cell bodies and dendritic processes (Figure 1, G

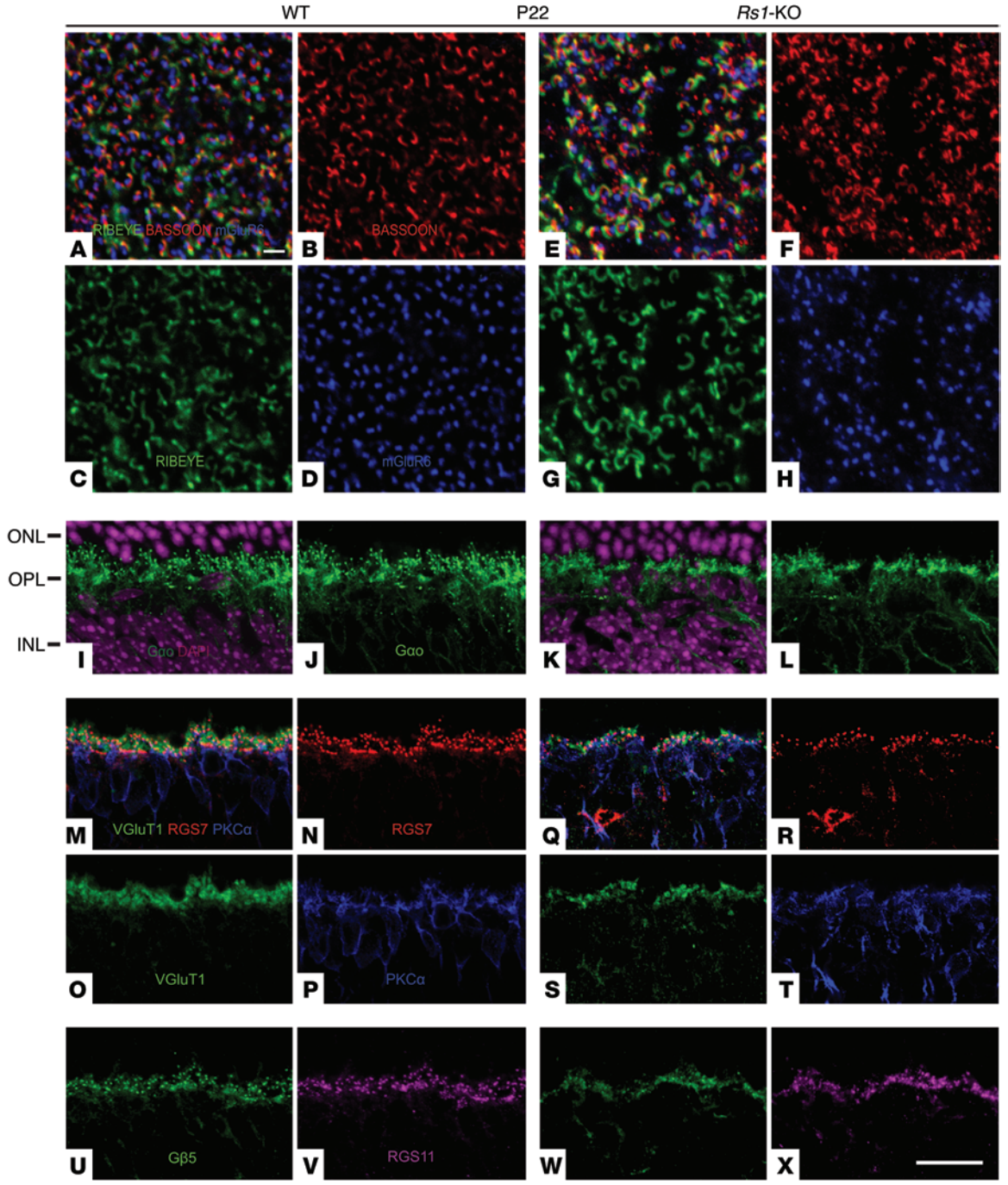

Figure 2. Photoreceptor-BC synaptic structure in WT and *Rs1*-KO retinas at P22. (**A**–**H**) En face image of whole-mounted WT (**A**–**D**) and *Rs1*-KO (**E**–**H**) retinas costained with antibodies against the presynaptic ribbon proteins RIBEYE (green) and Bassoon (red) and postsynaptic receptor protein mGluR6 (blue). Both WT and *Rs1*-KO retinas show normally intact rod photoreceptor active zones with horseshoe-shaped structures of RIBEYE and Bassoon, immediately adjacent to the mGluR6 receptor puncta specific for the dendritic tips of ON-BCs. At P22, Gαo proteins were normally concentrated at the dendritic tips and shafts (**I**, **J**), while *Rs1*-KO retinas had a grossly normal Gαo-staining pattern (**K**, **L**). Costaining of presynaptic VGluT1 (green), RGS7 (red) with PKCα (a marker for RBC; blue), and Gβ5 (green) with RGS11 (magenta) both showed similar patterns between WT (**M**–**P**, **U**, **V**) and *Rs1*-KO (**Q**–**T**, **W**, **X**) retinas. Scale bars: 2 μm (**A**–**H**); 20 μm (**I**–**X**). $n = 3$.

and I). In contrast, in *Rs1*-KO retina, dendritic staining for TRPM1 at the tips was greatly diminished even as staining of the soma remained evident (a typical pattern in the affected area is shown in Figure 1, H and J). Overall, TRPM1 signal intensity at DBC dendritic tips was approximately 36% of the total bipolar signal in *Rs1*-KO ($n = 5$), significantly lower than the 53% in WT (Figure 1N; $n = 5$; $P < 0.001$; Student's t test), or about two-thirds of normal. Consistent with reduced TRPM1 channels at the synaptic site, the membrane potential (MP) of rod BCs (RBCs; the predominant type of depolarizing ON-BCs in the mouse retina) in P22 *Rs1*-KO

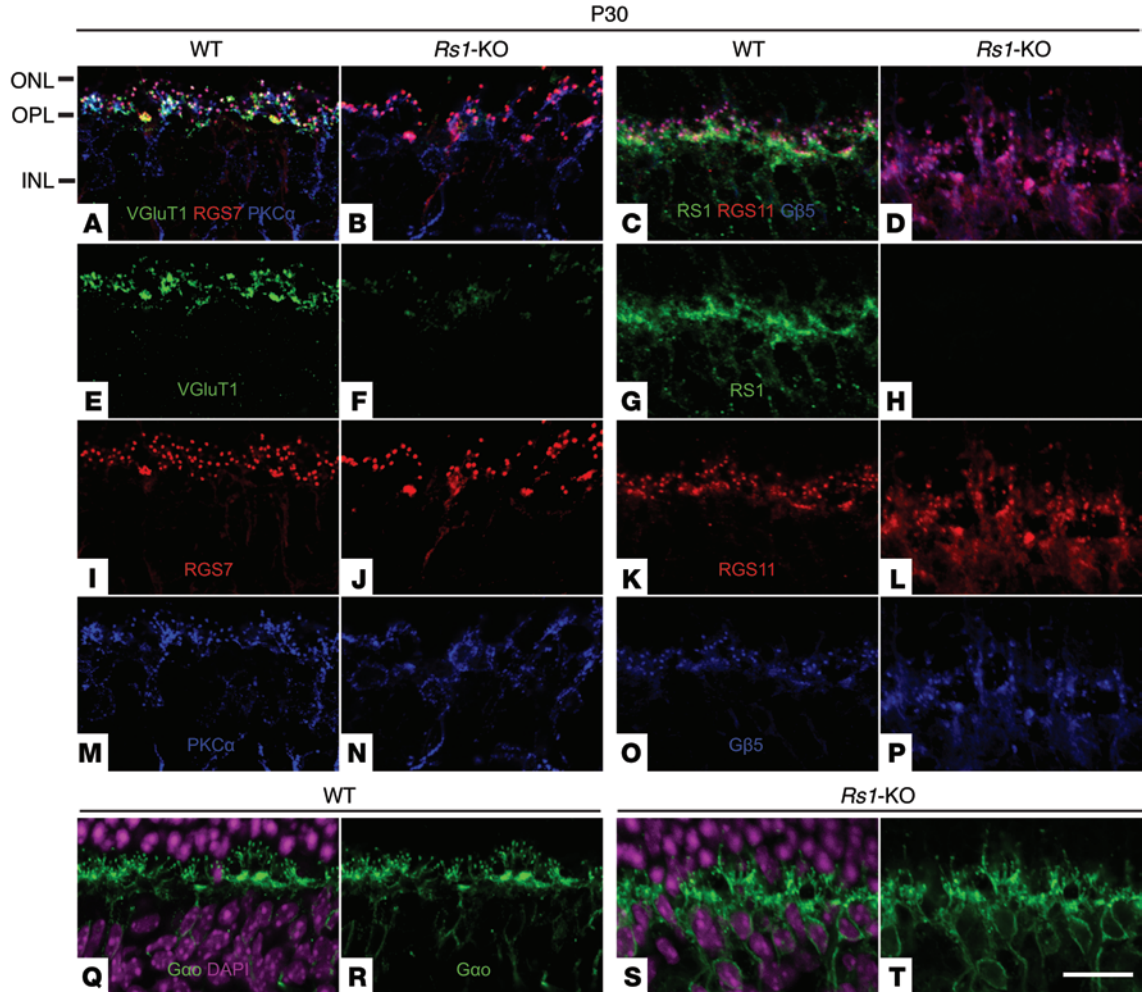

Figure 3. Deterioration of the mGluR6-signaling machinery in adolescent *Rs1*-KO mice. Gαo, Gβ5, RGS7, and RGS11 are key components of the glutamate-activated mGluR6-signaling machinery, and they appeared to be normal in expression levels and protein localization at P22 (see Figure 2, A–H, and Supplemental Figure 1). At P30, compared with WT (**A** and **E**), VGluT1 (green) proteins are no longer concentrated at the *Rs1*-KO photoreceptor synaptic terminals (**B** and **F**). Meanwhile, in both WT and *Rs1*-KO retinas, RGS7 (red) proteins are concentrated at the dendritic tips of the BCs counterstained with PKCα antibody (blue), even though the OPL and BCs have been disorganized in the mutant retinas (WT: **A**, **I**, and **M**; Rs1-KO: **B**, **J**, and **N**). Costaining of RS1 (green), RGS11 (red), and Gβ5 (blue) showed that at P30, in WT retinas (**C**, **G**, **K**, and **O**), RGS11 and Gβ5 proteins are mostly distributed to the ON-BC dendritic tips, with minor portions at the cell somas, while RS1 proteins remain at dendritic shafts. (**D**, **H**, **L**, and **P**) RS1 proteins have been absent in *Rs1*-KO retinas. In addition to the normal dendritic tip localization, RGS11 and Gβ5 proteins are prominently expanded toward the soma and axon of the BCs in *Rs1*-KO retinas (**L** and **P**). Compared with WT (**Q** and **R**), Gαo proteins in *Rs1*-KO retinas (**S** and **T**) also showed a prominent localization at the ON-BC somas and axons. Scale bars: 20 μm. $n = 3$.

mice was significantly hyperpolarized compared with that of WT (–37.0 ± 1.3 mV; $n = 5$ vs. –28.3 ± 1.4 mV; $n = 5$) (Figure 1O).

Failure of maintenance for synaptic connectivity. The expression pattern of the mGluR6-signaling cascade proteins Gβ5, RGS11, and RGS7 was more complex. These proteins regulate the open/closed state of TRPM1 channels via hydrolysis of Gαo-bound GTP to GDP (27). In P30 WT retina, RGS11 and Gβ5 were mostly restricted to bipolar dendritic tips (Figure 3, C, G, K, and O), but in *Rs1*-KO, they were beginning to be mislocalized and stream along the dendritic shaft to the soma (Figure 3, D, L, and P). RGS7, however, remained normally localized to the BC dendritic tips in *Rs1*-KO when counterstained with PKCα, a rod DBC marker (Figure 3, B, J, and N). Gαo (25), which was slightly reduced but with largely normal localization at BC dendrites in *Rs1*-KO at P22, showed a more prominent shift toward somal and axonal distribution at P30 (P22: Figure 2, I–L; P30: Figure 3, Q–T). Incipient mislocalization of RGS11 and Gβ5 was barely seen at P22 (Figure 2, U–X) and yet became more pronounced by P30 (Figure 3, K, O, L, and P). A similar and progressive reduction between P22 and P30 was found for VGluT1 (34). VGluT1 was sparsely present at photoreceptor terminals at P30 (Figure 3F), although earlier, at P22, the VGluT1-labeling pattern in the OPL appeared normal or only slightly reduced in *Rs1*-KO (Figure 2, M–T).

Plasticity and therapeutic repair of synaptic architecture and function by RS1 gene therapy. Recombinant AAV vectors were shown to mediate widespread delivery of the *RS1* gene to the outer retina and rescue the disease phenotypes of XLRS (17, 37–40). We used AAV8-mediated *RS1* gene transfer (AAV8-scRS/IRBP-*hRS1*, where IRBP indicates interphotoreceptor retinoid binding protein) to confer RS1 expression in *Rs1*-KO mouse retina. A dose of 2.5×10^9

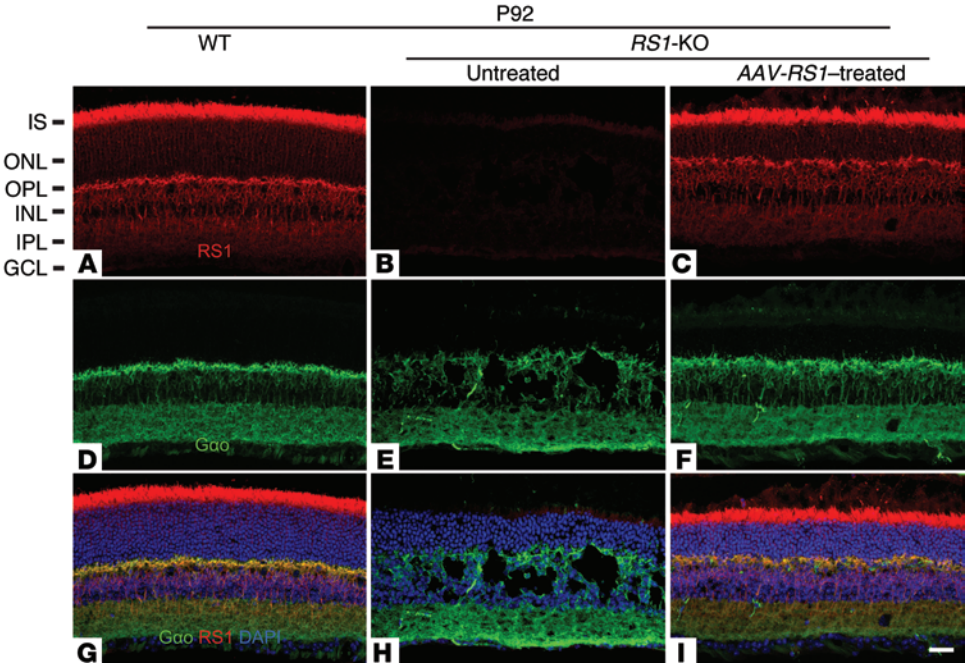

Figure 4. RS1 expression in AAV8-scRS/IRBP-*hRS1*–injected and uninjected *Rs1*-KO mice at 2 months after treatment (P92). Retinal sections from treated (right eye) and untreated (left eye) eyes of *Rs1*-KO mice 2 months after treatment, along with age-matched (P92) C57BL/6 WT mice were immunolabeled with anti-RS1 and anti-Gαo antibodies. *RS1* gene transfer into *Rs1*-KO mice retina leads strong expression of RS1 protein (red) in inner segments (IS) of photoreceptors and OPL similar to that seen in WT mouse retina (**A** and **C**). Labeling was also prominent, but to a lesser extent, in ONL, INL, and IPL. In treated retinas, BCs staining with Gαo (green) revealed absence of schisis and much organized BC layer arrangement (**F**) as in WT retina (**D**), whereas the untreated retinas from *Rs1*-KO mice showed no RS1 labeling and displayed schisis cavities and BC disorganization (**B** and **E**). (**G–I**) Gαo-RS1 overlay. Scale bars: 30 μm. $n = 3$.

viral vector genomes per eye was administered to *Rs1*-KO mice by intravitreal injection at P30, and its effect on the photoreceptor-DBC synaptic functions and structure 2 months after injection was assessed. The 24-kDa RS1-specific protein was present in multiple retinal layers from the AAV8-*RS1*–injected eyes, but absent in the contralateral controls, indicating that RS1 expression occurs upon treatment (Figure 4). The RS1 expression pattern was very similar to that seen in WT mouse retinas. While most intense staining was observed in the photoreceptor inner segment layer, it was also prominent within the OPL (Figure 4, A and C). RS1 labeling was also seen to a lesser extent in the outer nuclear layer (ONL), inner plexiform layer (IPL), and inner nuclear layer (INL). However, no significant difference in the thickness of the ONL was seen in the retinas of the treated eye compared with the untreated eye (Figure 4, H and I). With the disappearance of cavities following treatment, BCs (Gαo) in treated retina exhibited an organized arrangement of cells (Figure 4F) similar to that of WT retina (Figure 4D), whereas the untreated retina was disorganized and had substantial cavities across the retina (Figure 4E).

Two months after AAV8-*RS1* application, at P92, intracellular $[Ca^{2+}]i$ in photoreceptor presynaptic terminals of treated *Rs1*-KO retinas was restored to 69% of WT, whereas in untreated retinas, it was reduced further to 35% of WT (Figure 5A; $n = 4$; $P < 0.05$; Student's t test). Presynaptic VGluT1 showed robust staining in the OPL of treated eyes (Figure 5J), but was quite sparse in untreated retinas (Figure 5I). TRPM1 labeling at postsynaptic ON-BC dendritic tips of treated retinas, proximal to presynaptic marker RIBEYE (Figure 5, A–G), exhibited a significant increase, to 45%, of the total staining versus 37% in untreated *Rs1*-KO retinas (Figure 5, A–G; $n = 4$; $P < 0.001$; Student's t test). Concomitantly, the MP of ON-BCs was restored in treated *Rs1*-KO retinas (Figure 5A) to its normal depolarized state. ERG recording at P92 showed functional rescue with the ERG b-wave amplitude restored in treated eyes compared with the fellow control eyes (Figure 6A). These results indicate that photoreceptor–bipolar synapses maintained plasticity and that function was restored by AAV8-*RS1* gene transfer even at the P30 adult age after significant progression of synaptic pathology had occurred. Note that RS1 protein expression following gene transfer would be delayed by several to many days after vector delivery and that therapeutic action did not begin immediately upon injection at P30 (41).

The other postsynaptic signaling elements of the mGluR6-TRPM1 cascade were also restored to proper location by 2 months after AAV8-*RS1* delivery (Figure 7). In untreated P92 retinas, Gβ5, RGS11, and Gαo were further delocalized and streamed down the dendrite stalk and into the cell bodies. However, after treatment, they were relocalized and were tightly concentrated at ON-BC dendritic tips (Figure 7). In contrast to RGS11, Gβ5, and Gαo, both mGluR6 and RGS7 continued to be maintained at the dendritic tips in untreated *Rs1*-KO retina throughout this time, even at P92 (Figure 5, L and O), and following treatment, their densities were precisely aligned in the OPL zone of the synaptic layer (Figure 5, M and P). Both pre- and postsynaptic proteins were seen to be more organized and were tightly restricted in OPL lamination following AAV8-*RS1* delivery (Figures 5 and 7). As the ERG b-wave is generated by current flow through TRPM1 channels (22), we looked again at the response latency after provision of RS1 protein via the AAV8-*RS1* vector. Note that b-wave latency is also the implicit time of the a-wave trough after the ERG stimulus. The treated eyes showed orderly progression to shorter b-wave latency (a-wave implicit time) in dose-dependent fashion with the AAV8-*RS1* vector (Figure 6B). This is consistent with restoring the full set of signaling cascade proteins at the photoreceptor-BC synaptic zone.

Discussion

This study provides what we believe is new insight into the molecular and cellular pathological processes at the photoreceptor–ON–bipolar synapses in the mouse model (*Rs1*-KO) for human XLRS disease. Such synaptic dysfunction is in concord with the changes in ERG b-wave responses observed in *Rs1*-KO mice and human

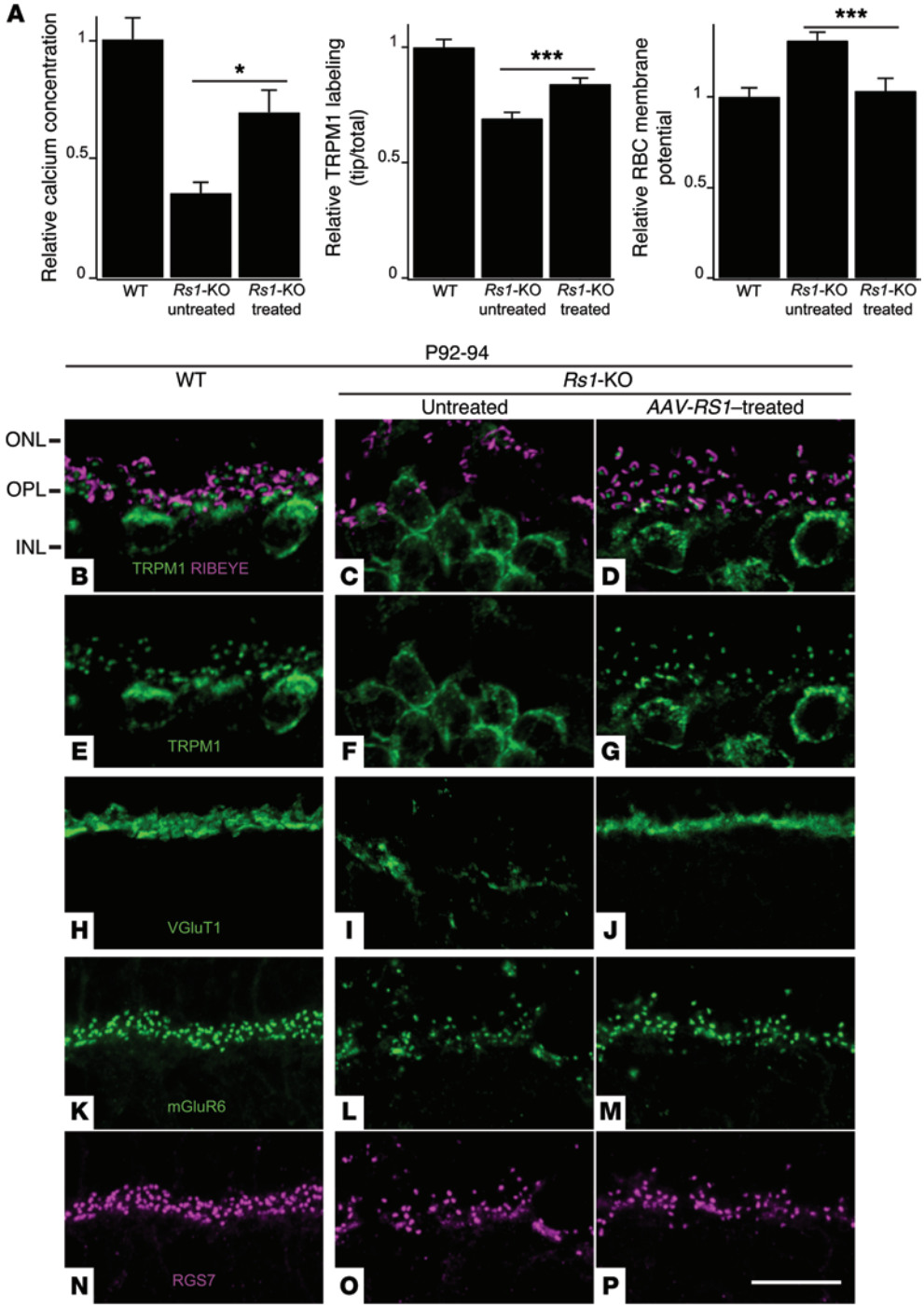

Figure 5. *RS1* gene transfer restores photoreceptor calcium homeostasis and TRPM1 functionality in *Rs1*-KO retinas. *Rs1*-KO retinas were injected with AAV8-scRS/IRBP-h*RS1* viruses at P30 and examined at P92. At P92, compared with WT retinas, the untreated *Rs1*-KO retinas had a disrupted OPL with scattered signals of RIBEYE (purple, **B** and **C**) and low abundance of the TRPM1 channel (green, **E** and **F**) at the OPL, while treated *Rs1*-KO retinas revealed improved lamination of the OPL and the close proximity of the presynaptic ribbon to the TRPM1 channels at the ON-BC dendritic tips (**D** and **G**). (**A**) Functional rescue by *RS1* gene transfer. Increases in rod photoreceptor synaptic free calcium concentration (untreated: 35% of that in WT; treated: 69% of that in WT [$n = 4$; $^*P < 0.05$, Student's t test]); TRPM1 intensity at ON-BC dendritic tips (percentage of whole-cell TRPM1 signal intensity; untreated: 37%; treated: 45% [$n = 4$; $^{***}P < 0.001$, Student's t test]); and light-adapted RBC MP: untreated retina –37 ± 1.4 mV vs. treated retina –29.2 ± 1.2 mV ($n = 4$; $^{***}P < 0.001$, Student's t test); WT retina –28.3 ± 1.4 mV. All *Rs1*-KO values were normalized to that of P30 WT. At P92, while VGluT1 (green) was localized at the OPL in WT retinas (**H**), it was scattered and less abundant at the disrupted OPL in untreated control retinas (**I**). Treatment led to a nearly normal appearance of VGluT1 immunoreactivity concentrated along the restored OPL of *Rs1*-KO retinas (**J**). Notably, the mGluR6 receptor (green) and RGS7 (purple) retained their normal localization at the ON-BC dendritic tips in *Rs1*-KO retinas regardless of the viral treatment (**K** and **N**: WT; **L** and **O**: untreated; **M** and **P**: AAV8-*RS1* treated). Scale bars: 15 μm (**B**–**G**); 20 μm (**H**–**P**). $n = 3$.

patients. Toward developing a therapeutic strategy, provision of RS1 protein via AAV8-mediated *RS1* gene transfer into adult *RS1*-KO mouse retina effectively reversed the pathological processes and greatly restored synaptic structure and function, which suggests a promising treatment outcome for patients with XLRS.

RS1 role in maintaining synaptic integrity. Although the development of the photoreceptor-BC synaptic architecture was largely intact in *Rs1*-KO mouse at age P22, both pre- and postsynaptic pathology were already evident. The TRPM1 channel was sparse in the postsynaptic dendritic tip, even though the mGluR6 receptor remained normal. In line with the defect in TRPM1 channels, the DBC membrane resting potential showed abnormal hyperpolarization. Concomitantly, in presynaptic photoreceptor terminals, intracellular $[Ca^{2+}]i$, which governs various aspects of neurotransmission, was also lower. Together, these pre- and postsynaptic defects led to reduced synaptic strength at an age before prominent retinal layer splitting occurs. Therefore, despite normal development, synaptic integrity was subsequently not properly maintained in the absence of RS1. As a result, RGS11, Gαo, and Gβ5 were progressively delocalized down the DBC dendrite stalk to the soma at P30 and even more so by P92. This synaptic failure underlies the progressively reduced ERG b-wave amplitude seen

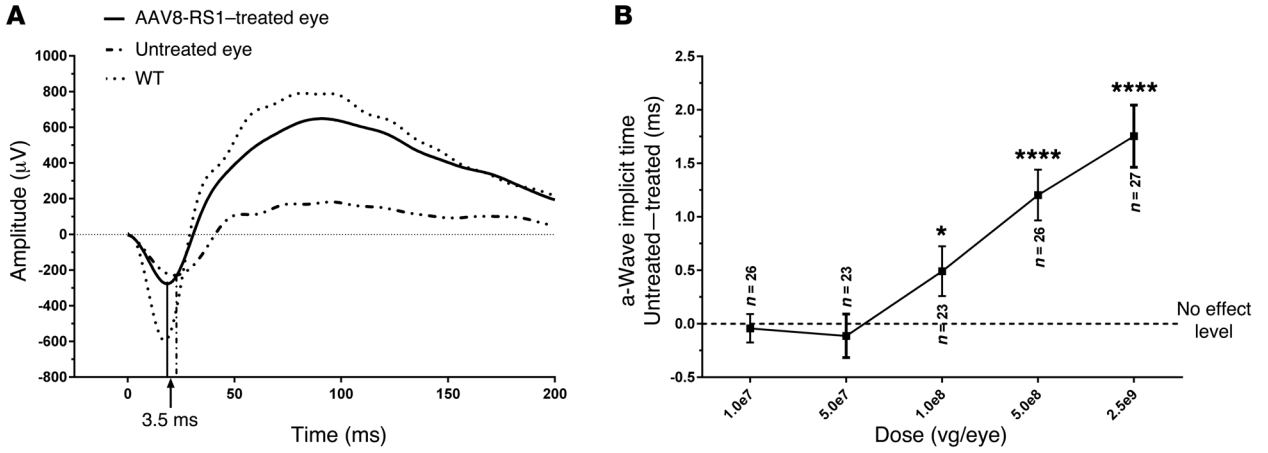

Figure 6. ERG in *Rs1*-KO mice showing that AAV8scRS/IRBP-h*RS1* gene transfer improves synaptic function. (**A**) Representative ERG waveforms (n = 3) from the treated and untreated eyes of an *Rs1*-KO mouse that received a unilateral injection of AAV8-scRS/IRBP-h*RS1* (2.5×10^9 vg/eye) at P30 compared with responses from a WT mouse. The dark-adapted ERG b-wave amplitude recorded from the untreated eye at P90 is decreased relative to the a-wave amplitude when compared with WT, indicating a reduced postsynaptic BC response to photoreceptor signaling. The AAV8scRS/IRBP-h*RS1*–treated eye, however, shows a selective improvement in b-wave amplitude, resulting in a waveform more similar to that of the WT. This indicates a restoration of postsynaptic responses. The a-wave amplitude is measured from baseline (0 ms) to the negative trough; b-wave amplitude is measured from the a-wave trough to the positive peak. Stimulus flash occurs at 0 ms. Arrows indicate the a-wave implicit time (time from stimulus flash to peak amplitude) for the treated and untreated eyes. (**B**) The a-wave implicit time for mice injected in 1 eye with 1 μl of AAV8-*RS1* at various doses or with 1 μl of vehicle. Values represent the average difference between the untreated and treated eyes (untreated – treated) at each dose. The a-wave implicit time is significantly shorter in treated eyes at doses of 1.0×10^8 vg/eye and higher. Asterisks indicate significance compared with zero, the value expected if there is no effect of treatment (*$P < 0.05$; ****$P < 0.0001$, 1-sample t test). n = 4.

in *Rs1*-KO mice (42) and in XLRS patients (43). Our results support the notion that RS1 plays an important role in maintaining the integrity of the photoreceptor–bipolar synapse.

Presynaptic versus postsynaptic defect. RS1 is expressed both presynaptically in photoreceptor terminals and postsynaptically in BCs, and it is difficult to differentiate whether the molecular changes in the BC dendritic tips are intrinsic or driven by photoreceptor pathology. Some mouse models in which mutations affect presynaptic release machinery, including Ca^{2+} channels (*CACNA1F*) and the synaptic ribbon (*BASSOON*; *RIBEYE*), result in postsynaptic changes secondary to the structural and functional defects of photoreceptor, such as dendrite sprouting and the formation of ectopic synapses by the bipolar and horizontal cell dendrites (44, 45). Similar observations are reported in the extreme case of very rapid photoreceptor degeneration in *rd1* mice (46). The decrease in photoreceptor synaptic terminal $[Ca^{2+}]i$ for *Rs1*-KO in this study and the presence of ectopic synapses in the ONL support the notion that presynaptic defects play an important role in the pathophysiology of XLRS (44, 47). This idea is consistent with a role of RS1 in maintenance of proper morphology and function of photoreceptors. Loss of RS1 expression is coincident with delayed maturation of photoreceptor (48). It is likely that a lack of RS1 compromises the membrane integrity of the photoreceptor inner segment and synaptic terminal, which in turn disrupts Ca^{2+} homeostasis by affecting the functions of membrane-embedded channels (e.g., other Ca^{2+} subunits) and ion pumps, including plasma membrane Ca^{2+} ATPase (PMCA). Consequently, perturbed Ca^{2+} homeostasis in photoreceptor synaptic terminals may contribute to photoreceptor degeneration (35).

One might reasonably assume that such presynaptic defects affect postsynaptic DBCs. Indeed, in *rd1* mice (PDE6b mutation), mGluR6 expression is reduced due to diminished presynaptic glutamate from loss of rod photoreceptors (46). This diminished mGluR6 signaling, as in *mGluR6*$^{-/-}$ mice, subsequently leads to reduced TRPM1 expression at DBC dendritic tips, similar to what has been observed in the *Rs1*-KO retina. Nonetheless, in the *Rs1*-KO mice, mGluR6 localization at dendritic tips is not affected, whereas TRPM1 is mislocalized and diminished even at an early age. Furthermore, elimination of mGluR6 in the *mGluR6*$^{-/-}$ mouse also reduces the signaling proteins RGS7 and RGS11 while preserving Gαo. This pattern does not fully overlap with *Rs1*-KO, in which Gαo is mislocalized, whereas RGS7 is not (Table 1). Thus, it is likely that the loss of RS1 alters postsynaptic architecture separate from or in addition to presynaptic changes, given that RS1 is expressed in both pre- and postsynaptic cells. RS1 protein previously was identified in the retinal BCs, even in *rd/rd c*1 mice of advanced age when no rod or cone photoreceptors are remaining (12). Our present studies refine this to show a relationship between RS1 and synaptic organization.

Genetic mutations of a number of these ON or DBC proteins cause synaptic failure with ERG b-wave abnormalities linked to the failure of DBC activity (19, 49). Defect in presynaptic release of glutamate and structural alterations in photoreceptor-DBC–to–BC synapse can also cause b-wave abnormalities and result in limited or no perception in dim light. These conditions are collectively termed CSNB and have a characteristic "electronegative" ERG waveform that retains the initial negative-going a-wave (from rod photoreceptor signaling), but lacks the following positive-going b-wave (involving postsynaptic DBC activity). However, we also note that none of the CSNB gene mutants and KO models of synaptic pathology in Table 1 exhibit a pattern identical to that found in *Rs1*-KO, which may reflect the difference between a primary

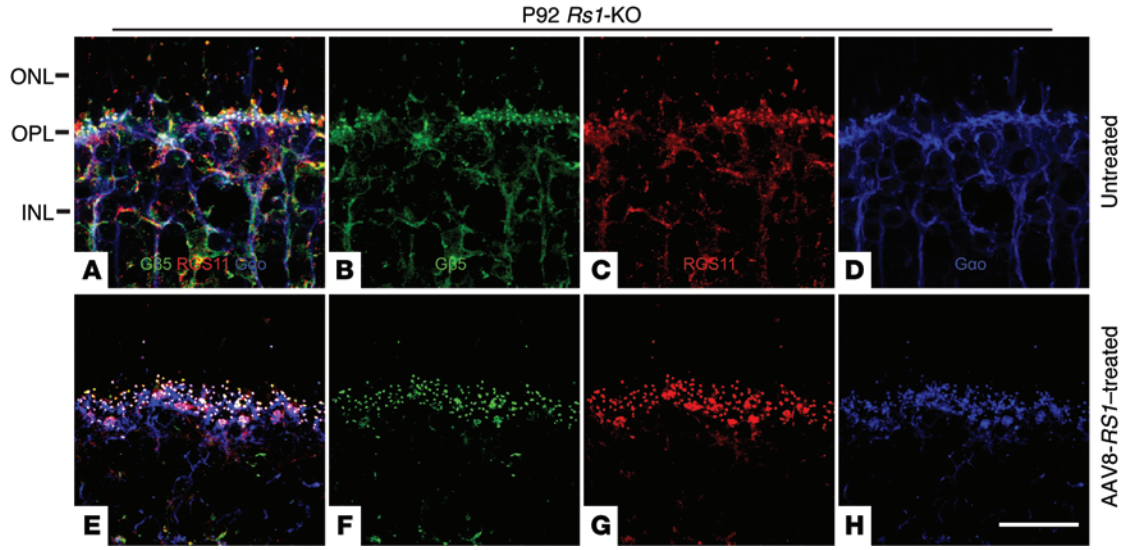

Figure 7. *RS1* gene transfer restores the normal mGluR6-signaling machinery in ON-BCs of *Rs1*-KO mouse retina. In addition to the restoration of the TRPM1 channel structure and functionality shown in Figure 5, costaining of Gβ5 (green), RGS11 (red), and Gαo (blue) of the mGluR6-signaling machinery revealed that, in untreated *Rs1*-KO retinas (**A**–**D**), together with the disrupted OPL, these proteins apparently diffuse toward the inner retina, while in AAV8-*RS1*–treated mutant retinas (**E**–**H**), concomitant with the restoration of the OPL, Gβ5, RGS11, and Gαo proteins appeared to have normal distribution in the BCs. Scale bars: 20 μm. $n = 3$.

loss of synaptic-signaling molecules versus ECM molecules, such as RS1, that are not directly involved in synaptic signaling.

TRPM1 channels. The loss of RS1 expression affects proper maintenance of TRPM1 channels at the BC dendritic tips in *Rs1*-KO. This finding is similar to that seen in *mGluR6*$^{-/-}$ and *Nyx*$^{-/-}$ retinas, which show reduced TRPM1 immunolabeling in dendritic tips, but not in the soma and primary dendrites (Table 1 and refs. 21, 29). However, *Trpm1*$^{-/-}$ mice have normal nyctalopin expression at the DBC dendrites, implying a more complex interaction involving additional proteins, such as a probable G protein–coupled receptor 179 (GPR179), which controls localization and activity of RGS complexes (50). Neither nyctalopin nor RS1 are directly linked to the transduction cascade, and how they affect the localization of membrane proteins at the synapse requires further study, with initial focus on cytoskeletal scaffolding proteins important for synaptic organization.

Loss of extracellular RS1 protein also affected presynaptic VGluT1 (which loads glutamate into synaptic vesicles) and postsynaptic RGS11, Gαo, and Gβ5, which progressively mislocalized to the soma beginning at P22 to P30 and progressing through P92. This corresponds well with progressive failure of ERG b-wave generation in XLRS disease (42, 43). RGS7, RGS11, and Gβ5 serve to accelerate GTP hydrolysis by Gαo and thereby set the time course of synaptic signaling. Mislocalization of these GTPase activity regulators was already evident by P30 and would affect the depolarized state of DBC (28, 32). The clinical corollary to RGS11 and Gβ5 mislocalization has been seen in human XLRS ERG as the delayed a-wave implicit time (i.e., the b-wave latency) of affected men (see Figure 5 in ref. 51). The progressive nature of XLRS disease in a mouse model is also reflected in an XLRS family with RS1-null protein expression, in which 2 young affected boys had developed nearly normal ERG b-wave amplitudes at a quite young age, but this was not maintained in their 4 XLRS male uncles, who had greatly diminished amplitudes by middle age (see Figure 4 in ref. 43).

AAV-mediated RS1 gene therapy. Feasibility of AAV-mediated gene therapy in an XLRS mouse model has been investigated by several groups. Zeng et al. (17) used AAV2-CMV-*Rs1h* delivered into the mouse vitreous and showed expression in all retinal layers and restoration of the ERG waveform in *Rs1h*-KO mice. Min et al. (37) used an AAV5 vector with the human RS1 cDNA and an opsin promoter, delivered into the subretinal space of *Rs1h*-deficient mice at P15, and achieved substantial RS1 expression in photoreceptors and the inner retina and rescue of rod and cone ERG responses for 5 months or more. This group also saw rescue when injecting as late as 7 months of age, by which time advanced disease had developed (38). Functional recovery, indicated by improved ERG b/a ratios, was recorded 11 weeks after injection. More recently (40), an AAV2 serotype variant vector with the opsin promoter and *RS1* gene gave rod-specific transduction in *Rs1*-KO mice and rescued morphology and function of the diseased retina when administered by vitreal delivery. Hence, rescue can be achieved by several routes of administration and by several AAV serotypes. In the present study, we used a self-complementary AAV8 construct (scAAV8) to shorten the expression delay and an IRBP enhancer sequence for robust *RS1* transgene expression. We chose the native RS1 promoter to restrict RS1 expression to photoreceptors, BCs, and other cells that normally express RS1 protein and to limit off-target expression (Figure 4).

Reorganization of the adult synapse following gene therapy. An intriguing aspect of the AAV8-*RS1* vector was the rapid rate of restructuring the signaling elements that are critical for synaptic signaling. The *RS1* gene was delivered at P30, and the molecular organization of both pre- and postsynaptic elements was largely restored to normal OPL localization at P92, including VGluT1, TRPM1, RGS11, Gβ5, and Gαo (Figures 5 and 7).

Proper alignment of TRPM1, RGS11, Gβ5, and Gαo at the synaptic site would facilitate the capacity of Gβ5, RGS11, and RGS7 to rapidly inactivate the G protein by accelerating GTP hydrolysis and thereby speed the generation of rod ON-BC light responses; this is reflected in shorter ERG a-wave trough/b-wave latency upon treatment (26, 27, 31). This confirms that RS1 plays a critical role in maintaining and reorganizing the synapse and demonstrates that the molecular architecture and function of the retinal synapse in the adult *Rs1*-KO animal remains plastic. This information is important for anticipating the timing of treatments for human patients.

The present study establishes criteria for RS1 as a synaptic cell-adhesion molecule in the retina: RS1 is present at the synapse; synapse formation in retinal layers is altered by loss of RS1 (4, 11); and restoring RS1 protein expression gives functional recovery and reorganization. Synapse organization involves physical attachment, and it is not surprising that an adhesion molecule such as RS1 would play a role in stabilizing a functional synapse and also in modulating experience-driven plasticity. Several synaptic cell-adhesion molecules and ECM components around the synaptic cleft facilitate the organization, alignment, and maturation of synaptic networks, and they are often referred to as synapse adhesion molecules (52–55). Many are members of the cadherin, integrin, and immunoglobulin super-families. Others include transmembrane heparin sulfate chondroitin sulfate proteoglycans (syndecan), ephrins, neuroligin, neurexin, and neuropilin. ECM molecules generally are transmembrane proteins with extracellular adhesion domains that assemble into repeating units. However, unlike conventional ECM molecules, RS1 lacks a transmembrane domain and is entirely extracellular, being secreted following synthesis and assembly into an octamer (56). As an octamer, RS1 can present multivalent adhesion interaction sites to the ECM through its discoidin domain motifs.

Although the precise biochemical mechanisms underlying RS1 function remain elusive, RS1 appears to have a cellular role independent of adhesion. Many RS1-interacting molecules, such as the β2 subunit of Na^+/K^+-ATPase complex (56), L-type voltage-gated calcium channel α1D subunit (L-VGCCα1D) (57), β2 laminin (58), anionic phospholipids (59), and galactose (60), have been identified, but the structural basis of their interactions remains to be determined. As RS1 is a lectin, its affinity to terminal sugars of a transmembrane glycoprotein might be a mode through which it can mediate intracellular signaling to modulate photoreceptor and BC functions. Molday's (56) proposal that binding of RS1 to Na^+/K^+-ATPase may influence fluid balance through an intracellular signaling pathway has some relevance in the context of retinal physiology and disease, but needs far more in-depth study to create a full understanding of the mechanism. Studies on the identification and characterization of the true in vivo RS1 ligand-receptor model would provide clues toward understanding RS1 function in photoreceptors.

In summary, this study highlights the role of RS1, an ECM protein in the maintenance of synaptic structure and function, as well as its ability to invoke synaptic plasticity and to restore structure and function when reintroduced in *Rs1*-KO mice. Because therapeutic intervention by gene delivery showed that synaptic disorders can be reversed in adult animals, this result offers hope that affected individuals may benefit from treatment even after symptoms set in. We are mounting a human trial with the same AAV8-*RS1* vector used in this murine study to probe synaptic plasticity in XLRS patients (ClinicalTrials.gov NCT02317887).

Methods

Animals. Male *Rs1*-KO mice and littermate WT controls were studied on P21–P22, P30–P32, and P90–P94. Animals were born and raised in our laboratory and derived from founders described by Zeng et al. (17). The *Rs1*-KO mice have been backcrossed onto C57BL/6J for more than 20 generations. They were raised in 20 lux lighting on a 12-hour light/12-hour dark cycle, with food and water available ad libitum. Animals were weaned at 3 weeks of age. All *Rs1*-KO mice in the study were genotyped from tail DNA to verify that they carried the *Rs1*-KO construct.

AAV8-RS1 gene vector and intravitreal injections. AAV8-scRS/IRBP-h*RS1* delivered a self-complimentary vector genome that contained human *RS1* gene-specific promoter, an IRBP enhancer, an intact human RS1 cDNA with a truncated first intron located in its authentic position between exon 1 and 2 sequences and a human β-globin 3′ UTR and polyadenylation site. This is the therapeutic vector we expect to use in the human clinical trial (ClinicalTrials.gov NCT 02317887). A dose of 2.5×10^9 viral vector genomes per eye was administered into the right eyes of 6 *Rs1*-KO mice by intravitreal injection at P30. The contralateral left eye served as the control and remained untouched. After anesthetizing animals with intraperitoneal ketamine (80 mg kg^{-1})/xylazine (15 mg kg^{-1}), both eyes of each mouse were dilated with 2.5% phenylephrine hydrochloride (Bausch & Lomb Inc.) and 0.5% tropicamide (Alcon Laboratories Inc.). Intravitreal injection was performed using a 5-μl Hamilton syringe with 33-gauge beveled-tip needle (Hamilton) inserted through the sclera just posterior to the limbus in the temporal side of the eye. Retinal morphology and functions were analyzed 2 months after injection. Untreated contralateral XLRS eyes served as controls.

Electroretinography. Retinal function was evaluated by recording the full-field scotopic ERG. Mice were dark adapted overnight and prepared under red dim light. They were anesthetized with intraperitoneal ketamine (80 mg/kg) and xylazine (10 mg/kg). Pupils were dilated with topical 0.5% tropicamide and 0.5% phenylephrine HCl. Body temperature was maintained at 37°C with a heating pad. ERGs were recorded from both eyes simultaneously. Gold wire recording loops were placed on the center of the cornea with a drop of methylcellulose for corneal hydration. A gold wire attached to the mouth was used as the reference electrode, and the common electrode was placed subcutaneously in the upper back. Scotopic responses were elicited using single flashes from −4.9 to +0.6 log cd•s/m2 in 0.5-log steps (Espion E2 System, Diagnosys LLC). Responses were computer averaged, with stimulus intervals of 3 to 60 seconds depending on stimulus intensity. The a-wave amplitude was measured from prestimulus baseline to the initial trough, and b-wave amplitude was measured from the a-wave trough. Separate measurements were made on 4 animals. ERG waveforms of a representative WT and *Rs1*-KO mice are shown.

Intracellular free [Ca^{2+}]i measurement. We measured intracellular free [Ca^{2+}]i in synaptic terminals of WT and *Rs1*-KO retinas. These experiments were performed under dim background illumination (mesopic range), in which calcium channels were likely to be submaximally activated. Buffers used in calcium-imaging assays are listed

in Supplemental Table 1. Mouse retinae were dissected, sliced, and incubated in Hibernate-A/B27 medium (Life Technologies) with 2.5 μM Fluo-4-AM dye (Life Technologies) at room temperature for 45 minutes. Excess dye was rinsed by 5% CO_2/95% O_2–saturated buffer containing 3 mM Ca^{2+}, and time-lapse $[Ca^{2+}]i$ imaging was performed and recorded on LSM510 confocal microscopy (ZEISS) with continuous irrigation. Rod photoreceptor synaptic terminals in-focus were identified and imaged before switching to 0 mM Ca^{2+} buffer containing 5 μM ionomycin (Sigma-Aldrich). After the fluorescent signals gradually decreased and stabilized, the buffer was switched to 20 mM Ca^{2+} with 5 μM ionomycin until the fluorescent signals reached maximum. The average intensities of fluorescence at 3 mM, 0 mM, and 20 mM Ca^{2+}buffer (F_3mM, F_0mM, and F_{20}mM) were obtained. The $[Ca^{2+}]i$ (nM) was calculated as follows: $[Ca^{2+}]i = Kd \times F_3mM - F_0mM)/(F_{20}mM - F_0mM)$. The average $[Ca^{2+}]i$ in *Rs1*-KO was normalized to that of WT.

Whole-cell recordings from BCs in retinal slice. All chemicals and reagents used in this study were obtained from Sigma-Aldrich except tetrodotoxin (TTX) (Abcam). During recording, dissected retina slices were perfused with bicarbonate-buffered Ame's media bubbled with 95% O_2 + 5% CO_2 at 32°C to 34°C. Picrotoxin (50 μM), (1,2,5,6-tetrahydropyridin-4-yl) methylphosphinic acid (TPMPA) (50 μM), strychnine (0.5 μM), and TTX (500 nM) were added to the Ames' media to block γ-amino butyric acid (GABAAR, GABACR), glycine receptors (GlyR), and voltage-gated Na^+ channel–mediated currents, respectively. The pipette solution contained the following: 108 mM potassium gluconate, 32 mM KCl, 0.5 mM $MgCl_2$, 10 mM HEPES, 2.5 mM K-EGTA, 3 mM ATP, and 1 mM GTP. The pH of the media was adjusted to 7.4 with KOH. Recordings were obtained with Axopatch 200B amplifiers (Molecular Devices). Data were digitized at 10 kHz using an ITC-18 interface (HEKA) controlled by a Dell computer running IgorPro 6.0 (WaveMetrics Inc.). MPs were recorded in whole-cell current clamp configuration immediately after break-in. Data were analyzed with custom-made software (IgorPro 6.0).

Immunohistochemistry. The retinas from WT and *Rs1*-KO mice were dissected, fixed in 4% PFA for 20 minutes, and either cut into smaller pieces for whole-mount staining or processed for either vibratome or cryosectioning by standard methods. Briefly, a high Triton X-100 (0.4%) containing PBS was used for permeating the retina pieces and a low Triton X-100 (0.1%) containing PBS (PBST) was used for retinal sections. Nonspecific binding sites in the tissue were blocked with 4% normal serum in PBST from the same host species as the labeled secondary antibody. Then primary antibodies with appropriate dilution in the serum-containing PBST buffer were added (antibodies and their dilutions used for immunohistochemistry are given in Supplemental Table 2). Whole-mount retinal tissues were incubated for 4 to 7 days, and retinal sections were incubated overnight. Subsequently, the retinal tissues or sections were washed with PBST at least 5 times for 20 minutes each time. Fluorescent secondary antibodies (Jackson ImmunoResearch Laboratories) were diluted 1:1000 in PBST and added to retinal whole-mount tissues or sections overnight or for 1 hour, respectively. Then the tissues or sections were washed in PBST and mounted. The sections were imaged on a Confocal Laser Scanning Module LSM 510 Microscope System (ZEISS). Images shown are representative of images obtained from retinas from at least 3 to 4 different animals for each genotype.

Western blotting. Retinas from WT or *RS1*-KO mice were lysed in RIPA buffer, pH 7.4 (50 mM Tris-HCl, 1% NP-40, 0.25% sodium deoxycholate, 150 mM NaCl, and 1 mM EGTA supplemented with Halt protease inhibitor cocktail; Thermo Fisher Scientific). Total protein was determined based on the bicinchoninic acid (BCA) method using the Pierce BCA Protein Assay Kit (Thermo Fisher Scientific). Retinal lysates (30 μg protein) were resolved on 10% Bis-Tris gels (Thermo Fisher Scientific) followed by blotting onto PVDF membranes by wet transfer. The membranes were blocked in blocking buffer (LI-COR Biosciences) and later incubated overnight with one of the indicated primary antibodies diluted in PBS containing 0.1% Tween 20 (PBST), pH 7.5, at 4°C. Antibodies and their dilutions used for Western blot are given in Supplemental Table 2. After overnight incubation, the membranes were rinsed 3 times in PBST and incubated with one of the following appropriate IRDye-conjugated secondary antibodies: IRDye 800CW-conjugated goat (polyclonal) anti-rabbit IgG or IRDye 800CW-conjugated donkey (polyclonal) anti-goat IgG (LI-COR Biosciences); or Alexa Fluor 680–conjugated goat anti-mouse IgG (Thermo Fisher Scientific). Blots were scanned on an LI-COR Odyssey Infrared Imaging System (Model 9120, LI-COR Biosciences) and analyzed using Odyssey software. Protein levels were normalized to β-actin signal.

Statistics. Data were statistically analyzed using Prism 5 (Graph Pad). Groups' differences were calculated by 2-tailed Student's *t* test or by 1-sample *t* test. Results are presented as mean ± SEM. *P* values of less than 0.05 were considered significant.

Study approval. The research involving animals was conducted in accordance with the Association for Research in Vision and Ophthalmology Statement on the Use of Animals in Ophthalmic and Vision Research. Prior approval for use of animals in this study was obtained from the Institutional Animal Care and Use Committee of the National Eye Institute (protocol number NEI-617). The NIH Institutional Biosafety Committee (IBC) approved the Human Pathogen Registration Document (HPRD no. 4766) and the Recombinant DNA Registration Document (RD-09-II-03).

Acknowledgments

We thank Jinbo Li, Maria Santos, and Suja Hiriyanna for technical assistance. We also thank the following for providing us with the antibodies used in this research: Takahisha Furukawa, the Osaka Bioscience Institute, Osaka, Japan (TRPM1); Catherine W. Morgans, Oregon Health & Science University, Portland, Oregon, USA (mGluR6); Theodore G. Wensel, Baylor College of Medicine, Houston, Texas, USA (Gβ5, RGS5, RGS7); K.A. Martemyanov, The Scripps Research Institute, Jupiter, Florida, USA (TRPM1); and Amy Lee, University of Iowa, Iowa City, Iowa, USA (CaV1.4). This work was supported by the Intramural Research Program of the NIH, the National Institute on Deafness and Other Communication Disorders, and the National Eye Institute.

Address correspondence to: Paul A. Sieving, National Eye Institute, 31 Center Dr., Bethesda, Maryland 20892, USA. Phone: 301.496.2234; E-mail: pas@nei.nih.gov.

Lucia Ziccardi's present address is: G.B. Bietti Foundation, IRCCS, Rome, Italy.

Jodie G. Pope's present address is: National Institute of Standards and Technology, Gaithersburg, Maryland, USA.

1. Jarraya B, et al. Dopamine gene therapy for Parkinson's disease in a nonhuman primate without associated dyskinesia. *Sci Transl Med*. 2009;1(2):2ra4.
2. Alexander B, et al. Reversal of depressed behaviors in mice by p11 gene therapy in the nucleus accumbens. *Sci Transl Med*. 2010;2(54):54ra76.
3. Akil O, et al. Restoration of hearing in the VGLUT3 knockout mouse using virally mediated gene therapy. *Neuron*. 2012;75(2):283–293.
4. Sikkink SK, Biswas S, Parry NR, Stanga PE, Trump D. X-linked retinoschisis: an update. *J Med Genet*. 2007;44(4):225–232.
5. Tantri A, et al. X-linked retinoschisis: a clinical and molecular genetic review. *Surv Ophthalmol*. 2004;49(2):214–230.
6. Haas J. Ueber das Zusammenvorkommen von Veranderungen der Retina und Choroidea. *Arch Augenheilkd*. 1898;37:343–348.
7. Pagenstecher H. Uebereine unterdem Bildeder Natzhauterblosung verlaufende, erbiche Erkankungder Retina. *Graefes Arch Clin Exp Ophthalmol*. 1913;86:457–462.
8. Thomson E. MEMORANDUM: Regarding a Family in which Neuro-Retinal Disease of an unusual kind occurred only in the Males. *Br J Ophthalmol*. 1932;16(12):681–686.
9. Sauer CG, et al. Positional cloning of the gene associated with X-linked juvenile retinoschisis. *Nat Genet*. 1997;17(2):164–170.
10. Gehrig AE, Warneke-Wittstock R, Sauer CG, Weber BH. Isolation and characterization of the murine X-linked juvenile retinoschisis (Rs1h) gene. *Mamm Genome*. 1999;10(3):303–307.
11. Weber BH, et al. Inactivation of the murine X-linked juvenile retinoschisis gene, Rs1h, suggests a role of retinoschisin in retinal cell layer organization and synaptic structure. *Proc Natl Acad Sci U S A*. 2002;99(9):6222–6227.
12. Molday LL, Hicks D, Sauer CG, Weber BH, Molday RS. Expression of X-linked retinoschisis protein RS1 in photoreceptor and bipolar cells. *Invest Ophthalmol Vis Sci*. 2001;42(3):816–825.
13. Grayson C, et al. Retinoschisin, the X-linked retinoschisis protein, is a secreted photoreceptor protein, and is expressed and released by Weri-Rb1 cells. *Hum Mol Genet*. 2000;9(12):1873–1879.
14. Genead MA, McAnany JJ, Fishman GA. Topical dorzolamide for treatment of cystoid macular edema in patients with choroideremia. *Retina*. 2012;32(4):826–833.
15. Genead MA, Fishman GA, Walia S. Efficacy of sustained topical dorzolamide therapy for cystic macular lesions in patients with X-linked retinoschisis. *Arch Ophthalmol*. 2010;128(2):190–197.
16. Khandhadia S, Trump D, Menon G, Lotery AJ. X-linked retinoschisis maculopathy treated with topical dorzolamide, and relationship to genotype. *Eye (Lond)*. 2011;25(7):922–928.
17. Zeng Y, et al. RS-1 gene delivery to an adult Rs1h knockout mouse model restores ERG b-wave with reversal of the electronegative waveform of X-linked retinoschisis. *Invest Ophthalmol Vis Sci*. 2004;45(9):3279–3285.
18. Jablonski MM, et al. An ENU-induced mutation in Rs1h causes disruption of retinal structure and function. *Mol Vis*. 2005;11:569–581.
19. Pardue MT, Peachey NS. Mouse b-wave mutants. *Doc Ophthalmol*. 2014;128(2):77–89.
20. Nomura A, Shigemoto R, Nakamura Y, Okamoto N, Mizuno N, Nakanishi S. Developmentally regulated postsynaptic localization of a metabotropic glutamate receptor in rat rod bipolar cells. *Cell*. 1994;77(3):361–369.
21. Xu Y, Dhingra A, Fina ME, Koike C, Furukawa T, Vardi N. mGluR6 deletion renders the TRPM1 channel in retina inactive. *J Neurophysiol*. 2012;107(3):948–957.
22. Koike C, et al. TRPM1 is a component of the retinal ON bipolar cell transduction channel in the mGluR6 cascade. *Proc Natl Acad Sci U S A*. 2010;107(1):332–337.
23. Morgans CW, et al. TRPM1 is required for the depolarizing light response in retinal ON-bipolar cells. *Proc Natl Acad Sci U S A*. 2009;106(45):19174–19178.
24. Peachey NS, et al. Depolarizing bipolar cell dysfunction due to a Trpm1 point mutation. *J Neurophysiol*. 2012;108(9):2442–2451.
25. Dhingra A, et al. The light response of ON bipolar neurons requires G[alpha]o. *J Neurosci*. 2000;20(24):9053–9058.
26. Rao A, Dallman R, Henderson S, Chen CK. Gβ5 is required for normal light responses and morphology of retinal ON-bipolar cells. *J Neurosci*. 2007;27(51):14199–14204.
27. Zhang J, et al. RGS7 and -11 complexes accelerate the ON-bipolar cell light response. *Invest Ophthalmol Vis Sci*. 2010;51(2):1121–1129.
28. Mojumder DK, Qian Y, Wensel TG. Two R7 regulator of G-protein signaling proteins shape retinal bipolar cell signaling. *J Neurosci*. 2009;29(24):7753–7765.
29. Pearring JN, et al. A role for nyctalopin, a small leucine-rich repeat protein, in localizing the TRP melastatin 1 channel to retinal depolarizing bipolar cell dendrites. *J Neurosci*. 2011;31(27):10060–10066.
30. Cao Y, Posokhova E, Martemyanov KA. TRPM1 forms complexes with nyctalopin in vivo and accumulates in postsynaptic compartment of ON-bipolar neurons in mGluR6-dependent manner. *J Neurosci*. 2011;31(32):11521–11526.
31. Morgans CW, et al. Gβ5-RGS complexes co-localize with mGluR6 in retinal ON-bipolar cells. *Eur J Neurosci*. 2007;26(10):2899–2905.
32. Cao Y, Pahlberg J, Sarria I, Kamasawa N, Sampath AP, Martemyanov KA. Regulators of G protein signaling RGS7 and RGS11 determine the onset of the light response in ON bipolar neurons. *Proc Natl Acad Sci U S A*. 2012;109(20):7905–7910.
33. tom Dieck S, et al. Molecular dissection of the photoreceptor ribbon synapse: physical interaction of Bassoon and RIBEYE is essential for the assembly of the ribbon complex. *J Cell Biol*. 2005;168(5):825–836.
34. Sherry DM, Wang MM, Bates J, Frishman LJ. Expression of vesicular glutamate transporter 1 in the mouse retina reveals temporal ordering in development of rod vs. cone and ON vs. OFF circuits. *J Comp Neurol*. 2003;465(4):480–498.
35. Krizaj D, Copenhagen DR. Calcium regulation in photoreceptors. *Front Biosci*. 2002;7:d2023–d2044.
36. Schweizer FE, Myers KM, Caputo A. In the zone: presynaptic function at high res. *Nat Neurosci*. 2012;15(7):928–929.
37. Min SH, et al. Prolonged recovery of retinal structure/function after gene therapy in an Rs1h-deficient mouse model of x-linked juvenile retinoschisis. *Mol Ther*. 2005;12(4):644–651.
38. Janssen A, et al. Effect of late-stage therapy on disease progression in AAV-mediated rescue of photoreceptor cells in the retinoschisin-deficient mouse. *Mol Ther*. 2008;16(6):1010–1017.
39. Park TK, et al. Intravitreal delivery of AAV8 retinoschisin results in cell type-specific gene expression and retinal rescue in the Rs1-KO mouse. *Gene Ther*. 2009;16(7):916–926.
40. Byrne LC, et al. Retinoschisin gene therapy in photoreceptors, Muller glia or all retinal cells in the Rs1h$^{-/-}$ mouse. *Gene Ther*. 2014;21(6):585–592.
41. Ali RR, et al. Adeno-associated virus gene transfer to mouse retina. *Hum Gene Ther*. 1998;9(1):81–86.
42. Kjellstrom S, Bush RA, Zeng Y, Takada Y, Sieving PA. Retinoschisin gene therapy and natural history in the Rs1h-KO mouse: long-term rescue from retinal degeneration. *Invest Ophthalmol Vis Sci*. 2007;48(8):3837–3845.
43. Vijayasarathy C, Ziccardi L, Zeng Y, Smaoui N, Caruso RC, Sieving PA. Null retinoschisin-protein expression from an RS1 c354del1-ins18 mutation causing progressive and severe XLRS in a cross-sectional family study. *Invest Ophthalmol Vis Sci*. 2009;50(11):5375-5383.
44. Johnson BA, Ikeda S, Pinto LH, Ikeda A. Reduced synaptic vesicle density and aberrant synaptic localization caused by a splice site mutation in the Rs1h gene. *Vis Neurosci*. 2006;23(6):887–898.
45. Chang B, et al. The nob2 mouse, a null mutation in Cacna1f: anatomical and functional abnormalities in the outer retina and their consequences on ganglion cell visual responses. *Vis Neurosci*. 2006;23(1):11–24.
46. Krizaj D, Huang W, Furukawa T, Punzo C, Xing W. Plasticity of TRPM1 expression and localization in the wild type and degenerating mouse retina. *Vision Res*. 2010;50(23):2460–2465.
47. Takada Y, Vijayasarathy C, Zeng Y, Kjellstrom S, Bush RA, Sieving PA. Synaptic pathology in retinoschisis knockout (Rs1–/y) mouse retina and modification by rAAV-Rs1 gene delivery. *Invest Ophthalmol Vis Sci*. 2008;49(8):3677–3686.
48. Ziccardi L, Vijayasarathy C, Bush RA, Sieving PA. Loss of retinoschisin (RS1) cell surface protein in maturing mouse rod photoreceptors elevates the luminance threshold for light-driven translocation of transducin but not arrestin. *J Neurosci*. 2012;32(38):13010–13021.
49. McCall MA, Gregg RG. Comparisons of structural and functional abnormalities in mouse b-wave mutants. *J Physiol*. 2008;586(pt 18):4385–4392.
50. Ray TA, et al. GPR179 is required for high sensitivity of the mGluR6 signaling cascade in depolarizing bipolar cells. *J Neurosci*. 2014;34(18):6334–6343.
51. Bowles K, et al. X-linked retinoschisis: RS1 mutation severity and age affect the ERG phenotype in a cohort of 68 affected male subjects. *Invest Ophthalmol Vis Sci*. 2011;52(12):9250–9256.
52. Missler M, Sudhof TC, Biederer T. Synaptic cell adhesion. *Cold Spring Harb Perspect Biol*. 2012;4(4):a005694.

53. Yamagata M, Sanes JR, Weiner JA. Synaptic adhesion molecules. *Curr Opin Cell Biol*. 2003;15(5):621–632.
54. Levy AD, Omar MH, Koleske AJ. Extracellular matrix control of dendritic spine and synapse structure and plasticity in adulthood. *Front Neuroanat*. 2014;8:116.
55. Kerrisk ME, Cingolani LA, Koleske AJ. ECM receptors in neuronal structure, synaptic plasticity, and behavior. *Prog Brain Res*. 2014;214:101–131.
56. Molday RS, Kellner U, Weber BH. X-linked juvenile retinoschisis: clinical diagnosis, genetic analysis, and molecular mechanisms. *Prog Retin Eye Res*. 2012;31(3):195–212.
57. Shi L, Jian K, Ko ML, Trump D, Ko GY. Retinoschisin, a new binding partner for L-type voltage-gated calcium channels in the retina. *J Biol Chem*. 2009;284(6):3966–3975.
58. Steiner-Champliaud MF, Sahel J, Hicks D. Retinoschisin forms a multi-molecular complex with extracellular matrix and cytoplasmic proteins: interactions with β2 laminin and αB-crystallin. *Mol Vis*. 2006;12:892–901.
59. Vijayasarathy C, Takada Y, Zeng Y, Bush RA, Sieving PA. Retinoschisin is a peripheral membrane protein with affinity for anionic phospholipids and affected by divalent cations. *Invest Ophthalmol Vis Sci*. 2007;48(3):991–1000.
60. Dyka FM, Wu WW, Pfeifer TA, Molday LL, Grigliatti TA, Molday RS. Characterization and purification of the discoidin domain-containing protein retinoschisin and its interaction with galactose. *Biochemistry*. 2008;47(35):9098–9106.